MOLECULAR PHYSICS, 1992, VOL. 75, NO. 3, 713–730

Non-equilibrium molecular dynamics simulations of structured molecules. II. Isomeric effects on the viscosity of models for *n*-hexane, cyclohexane and benzene

By RICHARD L. ROWLEY
Brigham Young University, Provo, Utah, 84602, USA

and JAMES F. ELY
National Institute of Standards and Technology†, Boulder, Colorado, 80303, USA

(*Received 29 May 1991; accepted 17 July 1991*)

The failure of extended corresponding-states techniques to predict the viscosity of low molecular weight branched and cyclic hydrocarbons suggests that molecular structure greatly affects the viscosities of these species. To investigate the inter-relationship of structure and viscosity, non-equilibrium molecular dynamics simulations of Lennard-Jones site–site models representing selected simple molecules were performed. The simulation conditions nearly span the liquid density range over which experimental data are currently available. In this study, models representing *n*-hexane, cyclohexane and benzene were constructed using six equivalent sites, each characterized by the same Lennard-Jones parameters used in a previous study of *n*-butane and isobutane viscosities. The focus was, therefore, entirely on structural effects. Simulated viscosities agreed well with experimental values of *n*-hexane and cyclohexane indicating that structural differences primarily account for the differences in viscosity between these two fluids. Simulated benzene viscosities were substantially higher than experimental values, indicating important non-structural effects. The relationship between fluid structure and the applied shear field are discussed.

1. Introduction

Extended corresponding states (CS) techniques such as TRAPP [1] and ELK [2] have proven to be very effective in the calculation of thermophysical properties of a wide range of fluids. In view of this general applicability, it is perhaps somewhat surprising that substantial errors result when these methods are used to calculate high-density liquid viscosities of the smallest branched and cyclical alkanes. This failure suggests a strong dependence of the viscosity on molecular structure for these molecules. We have, therefore, initiated a molecular dynamics (MD) study of the viscosity of model isomers and related compounds in an effort to elucidate some of the relationships between observed viscosity and molecular structure.

In a companion paper [3], simulations of *n*-butane and isobutane were performed. The fluids were modelled with four equivalent interaction sites connected by rigid bonds. In the case of *n*-butane, the torsional potential was modelled with the Ryckaert–Bellemans potential [4]. The simple structural differences between the models did not account for the difference in observed viscosity. In fact, the dimension-

† United States Government agency—this paper not subject to copyright in the United States.

0026-8976/92 $03.00

less viscosity of the branched model was lower than that of the normal alkane contrary to experiment. In the case of isobutane, scaling with respect to the Lennard-Jones (LJ) size parameter, σ, produces a considerably stronger influence on the viscosity than the structure, due to the σ^3 factor in the dimensionless number density. We found that an identical isobutane model with σ increased by only 2·5% from that used in the *n*-butane model produced excellent agreement with experiment. This is consistent with the idea that most of the intermolecular potential energy in isobutane is due to interactions between outer CH_3 groups rather than CH_2 groups. Jorgensen *et al.* [5] also found that spherically-averaged CH_3 groups required larger σ values than did the CH_2 groups when used in a group-contribution mode to calculate thermophysical properties from simulations. In view of the simplicity of these butane models, the excellent agreement obtained in [3] between simulated and experimental viscosities over the entire range of liquid densities accessible to the experimentalist is encouraging.

In this paper, we report MD studies performed on six-site models of C_6 fluids. Exactly the same site interactions are used here as in the previous *n*-butane simulations; this permits exclusive observation of structural effects. Models were chosen to represent the structure of *n*-hexane, cyclohexane and benzene, and simulated viscosities of these model fluids were compared to experimental data for the corresponding real fluids. It is important to stress that the model chosen is not the best one possible, but rather it represents the known structure of the fluid in terms of the same equivalent alkane-like site parameters. This is particularly true in the case of benzene for which more sophisticated models could be, and have been, constructed to account for effects of the π-cloud electrons. By consistently using the same site interactions, the structural effects on the viscosity can, however, be studied independent of other considerations. This is a distinct advantage of simulation, because a clean isolatation of structural effects from other inherent effects is not possible in an experimental comparison of real fluid viscosities.

2. Molecular models

2.1. *n-Hexane*

The effective site–site model for alkanes used by Ryckaert and Bellemans to model *n*-butane [6] and *n*-decane [4] has been shown to work well for predicting thermophysical properties of normal alkanes in a number of simulation studies. The *n*-alkane model molecule is composed of equivalent methyl–methylene sites located at carbon centres. Intermolecular sites, as well as intramolecular sites separated by more than three sites, are assumed to interact with Lennard-Jones (LJ) potentials. Interactions between different molecules are then represented as the pairwise-additive sum of all possible site–site interactions. Figure 1 shows the geometry and the characteristic parameters of the model. Values of these parameters are contained in table 1. The

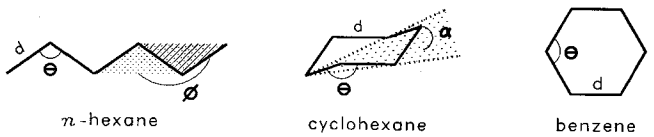

Figure 1. Fixed bond-length and bond-angle models for *n*-hexane, cyclohexane and benzene identifying the structural parameters for which values are reported in table 1.

Table 1. Model parameters.

Parameter	Units	*n*-hexane	Cyclohexane	Benzene
m (site mass)	kg	$2{\cdot}385 \times 10^{-26}$	$2{\cdot}329 \times 10^{-26}$	$2{\cdot}162 \times 10^{-26}$
d (bond distance)	nm	0·153	0·154	0·1397
Θ (bond angle)	degrees	109·47	109·47	120·0
ε/k (LJ energy parameter)	K	72	72	72
σ (LJ distance parameter)	nm	0·3923	0·3923	0·3923
ϕ (dihedral angle)	degrees	variable	—	—
α (out of plane angle)	degrees	—	35·36	0·00

bond lengths and bond angles are constrained by the simulation to the values shown in table 1. The three dihedral angles in the *n*-hexane model—shown in figure 1 as the angle ϕ between the shaded planes—are allowed to vary in accordance with the Ryckaert–Bellemans intramolecular potential,

$$\frac{U(\phi)}{k} = \sum_{k=0}^{5} a_k \cos^k \phi. \tag{1}$$

Values of the potential parameters were determined from *n*-butane by Ryckaert and Bellemans [6] to be 1116, 1462, −1578, −368, 3156 and −3788 K for a_0 to a_5, respectively. These values have been used effectively in simulations of other alkanes [4, 7–9]. The values of σ and ε used in this work are the same as those used by Edberg and Evans [7, 8] in their simulations of *n*-butane and *n*-decane viscosities. These same values produced excellent agreement with experimental viscosities for *n*-butane in [3]. Brown and Clarke [9] have also performed simulations of *n*-hexane using this model at a single temperature and density. They used the same value of σ as we do, but their value of ε was about 16% higher. As shown in [3], the simulated viscosity is very sensitive to the value of σ chosen due to the σ^3 scaling of the reduced density. Conversely, the viscosity is relatively insensitive to the value chosen for ε. This roughly corresponds to the experimental observation that viscosity is a strong function of density, but only a weak function of temperature at constant density.

2.2. *Cyclohexane*

Pickett and Strauss [10] proposed a rather ingenious coordinate system for cyclohexane and other non-planar, cyclic models which allowed them to identify conformational interconversion in terms of only two coordinates. They also developed an intramolecular potential model in terms of these coordinates that allowed them to map the conformational energies. Kuharski *et al.* [11] used a modified Pickett–Strauss model in their stochastic MD study of cyclohexane isomerization. Pickett–Strauss used rigid C–C bond lengths of 0·154 nm while Kuharski *et al.* included vibrational motion about the equilibrium bond length of 0·154 nm. Hoheisel and Würflinger [12] used a similar six-site model with bond lengths of 0·154 nm constrained in the chair conformation to perform MD simulations of thermodynamic and transport properties. For the chair configuration they used the tetrahedral angle and regressed the values of $\varepsilon/k = 78$ K and $\sigma = 0{\cdot}386$ nm for the LJ site parameters from experimental thermodynamic data. Interestingly, they reported that the simulated equilibrium properties were 'acceptable' although the density dependence was slightly wrong and that the transport properties *except* viscosity agreed well. The simulated viscosities were found to be 'appreciably larger' than experimental values.

We retain the six-equivalent-site model used in these previous studies. The model and appropriate defining parameters are shown in figure 1. Values of these parameters used in the simulations are reported in table 1. Our interest in isolating the purely structural effects on viscosity required that the values of ε/k and σ used for the sites be the same as for the *n*-hexane model, and the model was 'frozen' in the chair conformation. The LJ site parameters are not identical with those used by Hoheisel and Würflinger, but are quite similar. The C–C bond distance was constrained at the equilibrium bond lengths and the bond angles were taken as the tetrahedral angle as in previous studies. The internal angle, α, used by Kuharski *et al.* and Pickett and Strauss, measures the non-planar character of the model (see figure 1). For the ideal chair conformation, all three angles α are set to 35·36° [10].

2.3. *Benzene*

The structural properties of benzene have been fairly extensively simulated using different intermolecular potential models of varying complexity [13–23]. Evans and Watts [13] used a six LJ site potential with centres located midway on the C–H bonds. Steinhauser [14] used a similar six-site model, but with the centres located at the carbon atoms. Ryckaert and coworkers [15, 16] used the same LJ potentials as Evans and Watts with the addition of a point quadrupole at the centre of the molecule. Linse and coworkers [17, 18] used 12-site models with point charges located at the C and H atoms with parameters obtained from earlier *ab intio* calculations [19]. This same *ab initio* potential was used by Maliniak and Laaksonen [20]. Yashonath *et al.* [21] also used six- and twelve-site models with electrostatic contributions at the sites. Anderson *et al.* [22] used a combination of *ab initio* intramolecular interactions with semi-empirical atom–atom intermolecular potentials. Gupta *et al.* [23] used a modified gaussian overlap potential as well as six-site potential models. These simulations have demonstrated that the electrostatic interaction between benzene molecules is an important factor in determining accurate fluid and solid properties. Models using six equivalent LJ sites have been shown to favour a stacked structure in which molecules lie one above another, imparting more short-range order than experimental evidence would dictate. The stacked configuration is destabilized by the introduction of a point quadrupole interaction located at the centre of the molecule, but can produce unsatisfactory results for the structure of the solid phase. The increasingly complex models generally yield improved simulated properties for both the liquid and solid phases.

These, and other studies, have focused primarily on the structure of the fluid and solid and equilibrium properties. We use in this work a six-site model with the interaction sites located at C centres. The bond lengths are fixed at 0·1397 nm which corresponds to the accepted experimental value [23]. The geometry is considered to be that of a planar regular hexagon. Again, appropriate model parameters are depicted in figure 1 and their values given in table 1. While the LJ parameters were purposely fixed at the same values as used in the *n*-hexane and cyclohexane simulations, they are quite similar to those used in the above-mentioned specific studies of benzene. The previously noted limitations of the six-site model are expected to affect the values of the simulated viscosities; this is in fact by intent. As mentioned, we seek not to find the most accurate model for simulating benzene viscosities, but desire to study the difference in simulated viscosity for structural models representing the *geometry* of the three different fluids with the same LJ parameters.

3. MD Simulations

Non-equilibrium MD simulations were performed using an NVT (canonical ensemble) algorithm developed by Edberg *et al.* [7], a molecular version of the isothermal shear algorithm known as SLLOD [24, 25]. Rather than solve Newtonian equations of motion subject to constraints as popularized by the SHAKE algorithm [26], non-Newtonian equations of motion which naturally include the constraint forces are derived following the prescription of Gauss's principle of least constraint [7, 25, 27]. A principal advantage of this method for the type of problem considered here is that all of the constraints imposed by the fixed bond distances, the thermostat and the applied shear field are similarly and efficiently incorporated into the equations of motion as additional force terms. This makes implementation of the method into standard MD programs relatively straightforward. Newtonian forces $\boldsymbol{F}^{\mathrm{N}}$ can be

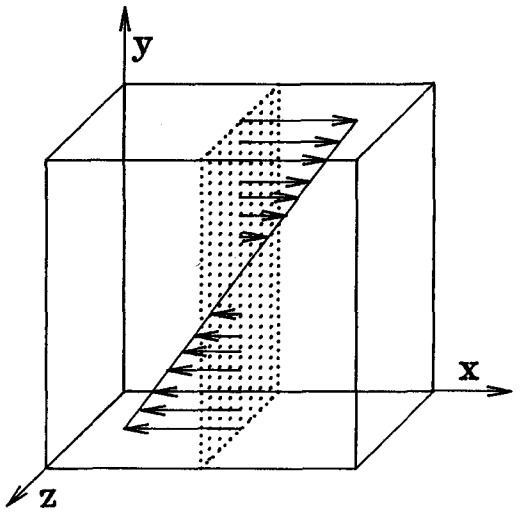

Figure 2. Schematic showing the linear velocity profile or constant shear rate in relation to the coordinate system used in the simulations.

calculated from relative site positions in the standard way, the constraint forces $\boldsymbol{F}^{C}$ can be obtained from Gauss's principle, and the usual integration algorithms may be used to trace the particle trajectories in phase space using the total force, $\boldsymbol{F}^{N} + \boldsymbol{F}^{C}$. Derivation of the appropriately constrained equations of motion and their implementation into standard MD codes are adequately discussed in [3, 7, 8, 28].

NVT simulations were performed on three-dimensional systems of 125 molecules using a cut-off distance of $2{\cdot}5\,\sigma$ with appropriate long-range corrections. The geometry used is schematically shown in figure 2 and the constant applied shear rate γ in the simulations is defined with respect to these cartesian coordinates and the x component of velocity as

$$\gamma = \left(\frac{\partial v_x}{\partial y}\right). \tag{2}$$

All simulations were performed on a Cyber* 205 supercomputer using the automatic vectorization options of the resident FORTRAN compiler. The dimensionless time step size was chosen to be 0·0015, corresponding to about 2·9 fs in real time. Between 60 000 and 120 000 time steps beyond 'equilibration' were used to obtain property time averages. All production runs were started from configuration files of previous simulations by changing the run conditions or shear rate. This generally shortened the time required to 'equilibrate', or stabilize the simulated properties, to about 20 000 time steps. The simulation code is essentially that described [3]. Briefly, it is the code used by Edberg and Evans streamlined with a neighbourhood list and multiple time steps in order to make the quantity of computations required in this study feasible. Details are provided in [3], and the bond constraint matrices used for the C_6 fluids studied here are given in the Appendix.

As in [3], bulk properties of the fluid were computed with the standard time

*Brand names and commercial sources of materials and instruments are given for scientific completeness and comparison purposes. Such information does not constitute endorsement of these products or imply their superiority over other available brands.

Table 2. Approximate numerical relationships between dimensionless and experimental variables.

Property	Relationship
Temperature	$T^* = T/(72\,\mathrm{K})$
Molar density	$\rho^* = \rho_m/(4{\cdot}6\,\mathrm{mol\,dm^{-3}})$
Shear rate	$\gamma^* = \gamma/(5 \times 10^{11}\,\mathrm{s^{-1}})$
Viscosity	$\eta^* = \eta/(0{\cdot}03\,\mathrm{mPa\,s})$
Time	$t^* = t/(1{\cdot}93\,\mathrm{ps})$

averages of appropriate dynamical variables. The shear-dependent viscosity, $\eta(\gamma)$, was computed from the molecular pressure tensor as before. Extrapolation of $\eta(\gamma)$ to zero shear yields the Green–Kubo viscosity, $\eta(0)$. This extrapolation is done using

$$\eta(\gamma) = \eta(0) - A\gamma^{1/2}. \tag{3}$$

Simulations were performed along isotherms at densities corresponding to those of available experimental data [29–31]. Properties were made dimensionless in terms of site parameters, thus,

$$T^* = \frac{kT}{\varepsilon}, \qquad \eta^* = \eta\sigma^2/(m\varepsilon)^{1/2}, \qquad \gamma^* = \gamma\sigma\left(\frac{m}{\varepsilon}\right)^{1/2}. \tag{4}$$

Likewise, the site number density, ρ, is six times the molecular number density, or

$$\rho^* = \rho\sigma^3 = \frac{6N\sigma^3}{V}. \tag{5}$$

Approximate numerical relationships between dimensionless and experimental variables applicable to this work are given for convenience in table 2.

4. Results and discussion

Simulations were planned for all three models at four different densities which nearly span the range of experimentally available data for liquids. At each state point, simulations were made at four different shear rates to permit extrapolation of η^* to zero shear. Shown in figures 3 to 5 are the results of the shear dependent values of η^*. Block averages of η^* indicate that the uncertainties in these points become large very rapidly as the applied shear rate is reduced below a γ^* of 0·04. Standard deviations obtained from block averages generally overestimate the uncertainty in simulated values and therefore are not included in figures 3 to 5, but their relative values at each state point were used to determine the weights used in a non-linear regression program to extrapolate η^* to $\gamma^* = 0$. As shown in these figures, simulation values agree well with the linear relationship of (3). The points shown at $\gamma^* = 0$ are the regressed intercepts, not simulation results.

The results of these simulations, the values obtained by extrapolation to zero shear, and experimental values at the same temperature and density are given in table 3. A comparison of the simulation results for the model fluids to experimental data is shown in figures 6 and 7.

Figure 6 compares the simulated viscosities for model *n*-hexane and cyclohexane molecules to experimental values over a wide density range. The excellent agreement with experiment indicates two things to us. (1) Simple n_s site–site models of alkanes containing n_s carbons are quite efficacious in predicting pure fluid viscosities over

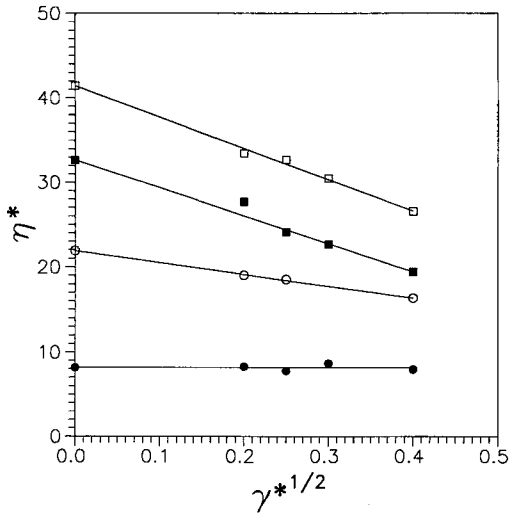

Figure 3. Results of *n*-hexane simulations for $\eta^*(\gamma^{*1/2})$ at $T^* = 4{\cdot}141$ and $\rho^* = 1{\cdot}661$ (●), $\rho^* = 1{\cdot}863$ (○), $\rho^* = 1{\cdot}929$ (■) and $\rho^* = 1{\cdot}995$ (□). Lines represent weighted least squares fits through data shown.

virtually the entire liquid domain. We base this conclusion not just on the results obtained here for *n*-hexane and cyclohexane, but also the excellent agreement obtained for *n*-butane and isobutane in [3]. (2) The difference in viscosity between liquid *n*-hexane and cyclohexane is primarily geometrical in nature. The structural difference between the chain and ring models does account for the observed difference in experimental viscosities as evidenced by the excellent agreement with experiment for both geometrical models. Evidently there is little or no inherent difference between the cyclic and chain CH_2 sites, at least with respect to their effects upon the viscosity.

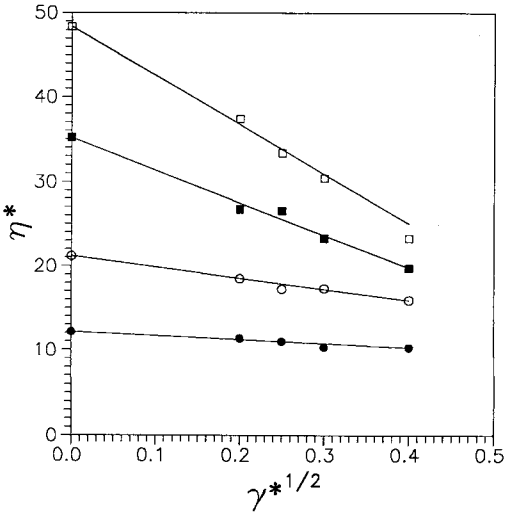

Figure 4. Results of cyclohexane simulations for $\eta^*(\gamma^{*1/2})$ at $T^* = 5.319$ and $\rho^* = 1{\cdot}863$ (●), $\rho^* = 2{\cdot}012$ (○), $\rho^* = 2{\cdot}092$ (■) and $\rho^* = 2{\cdot}155$ (□). Lines represent weighted least squares fits through data shown.

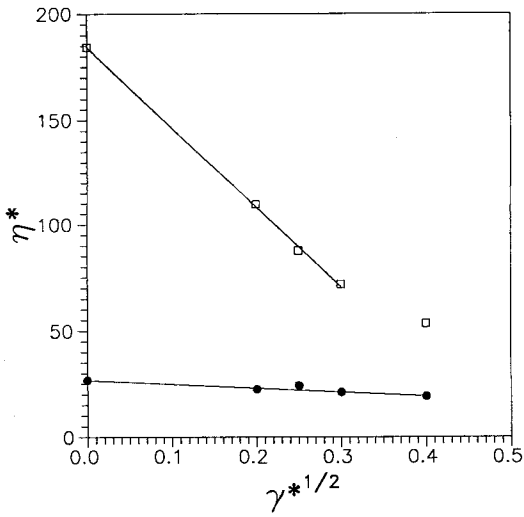

Figure 5. Results of benzene simulations for $\eta^*(\gamma^{*1/2})$ at $T^* = 5.183$ and $\rho^* = 2{\cdot}210$ (●) and $\rho^* = 2{\cdot}528$ (○). Lines represent weighted least squares fits through data shown.

This is different than the observation in [3] in which the difference in geometry between *n*-butane and isobutane did not adequately explain the differences in observed viscosity. In that case, we found that the presence of three CH_3 groups and a single CH site required a larger effective σ value than for the straight-chain isomer. As mentioned, a change of only 2·5% in σ shifted the ρ^* values enough to bring the simulated values into agreement with experiment.

Simulated values for the structural analogue of benzene do not compare well with actual experimental data as can be seen in figure 7. This was somewhat expected in light of previous equilibrium studies of the local structure that showed an artificial

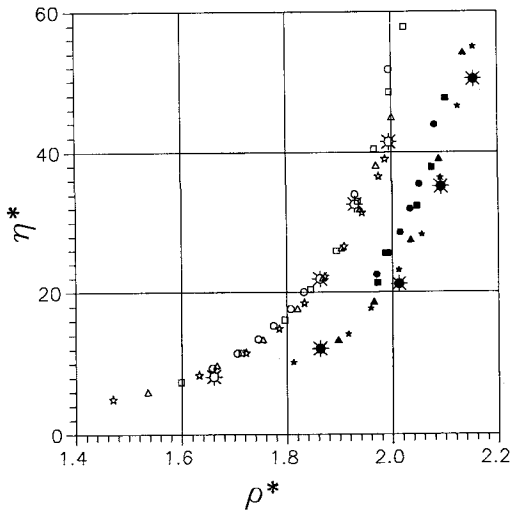

Figure 6. Comparison of simulated (larger symbols with radial lines) and experimental (smaller symbols) reduced viscosities for *n*-hexane (open symbols) and cyclohexane (full symbols). Different smaller symbols indicate different experimental isotherms.

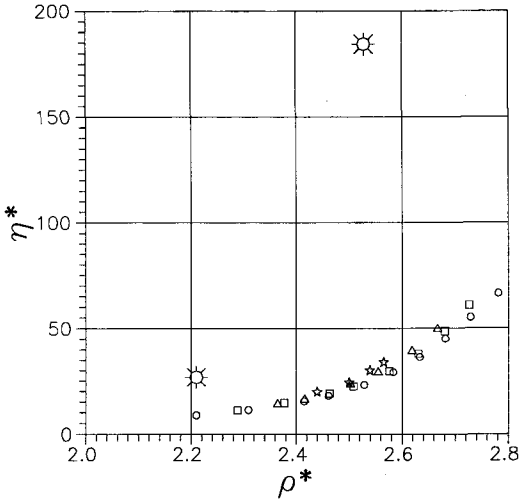

Figure 7. Comparison of simulated (larger symbols with radial lines) and experimental (smaller symbols) reduced viscosities for benzene. Different smaller symbols indicate different experimental isotherms.

stacking of the benzene molecules when a six-site model without a point quadrupole was used. We were surprised, however, at the magnitude of the difference. In fact, we completed only two of the four planned simulations for model benzene because of the very rapid increase in viscosity that occurs at much lower densities than observed experimentally. This behaviour is consistent with a scaling problem, but might also be attributed to the lack of point quadrupole. ρ^* scales with σ^3, thus relatively small changes in σ can mean a large difference in the corresponding dimensionless density. If σ is too large, then the simulations are performed at a much higher density than the corresponding experiments and the steep rise in η^* with ρ^* would occur at much lower densities, consistent with the trends observed in figure 7. This is not the only possible explanation, but any explanation supports the primary finding that the planar struc-

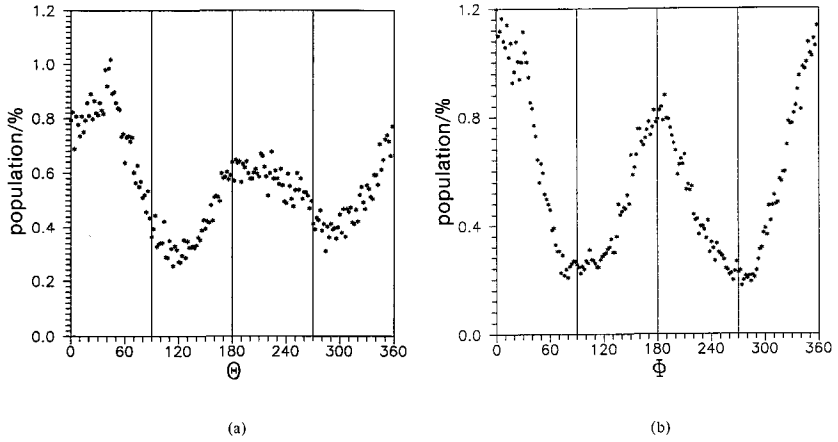

Figure 8. Histogram of percentage population of *n*-hexane molecules at $\rho^* = 1{\cdot}995$ and $\gamma^* = 0{\cdot}16$ whose orientation vector $\boldsymbol{b}$ and the x-axis form an angle (*a*) Θ in the x–y plane and (*b*) Φ in the x–z plane.

Table 3. Results of simulations.

	T^*	ρ^*	η^* $\gamma^* = 0{\cdot}16$	η^* $\gamma^* = 0{\cdot}09$	η^* $\gamma^* = 0{\cdot}0625$	η^* $\gamma^* = 0{\cdot}04$	$\eta^*(0)$ (sim)	η^* (exp)
Hexane	4·141	1·661	7·96	8·68	7·79	8·28	8·18	9·21
	4·141	1·863	16·36	—	18·54	19·03	21·91	21·38
	4·141	1·929	19·46	22·64	24·12	27·66	32·63	33·86
	4·141	1·995	26·57[a]	30·46[a]	32·64	33·44	41·41	51·44
Cyclohexane	5·319	1·863	10·25	10·31	10·98	11·38	12·16	12·22
	5·319	2·012	15·94	17·35	—	18·50	21·19	23·16
	5·319	2·092	19·76	23·29	26·57	26·71	35·16	36·37
	5·319	2·155	25·32	30·43	33·27	37·40	48·36	54·93
Benzene	5·183	2·210	19·12	21·13	24·22	22·49	26·79	8·79
	5·183	2·528	53·53	71·86	87·67	109·72	184·24	23·14

[a] Value not used in extrapolation to $\gamma = 0$.

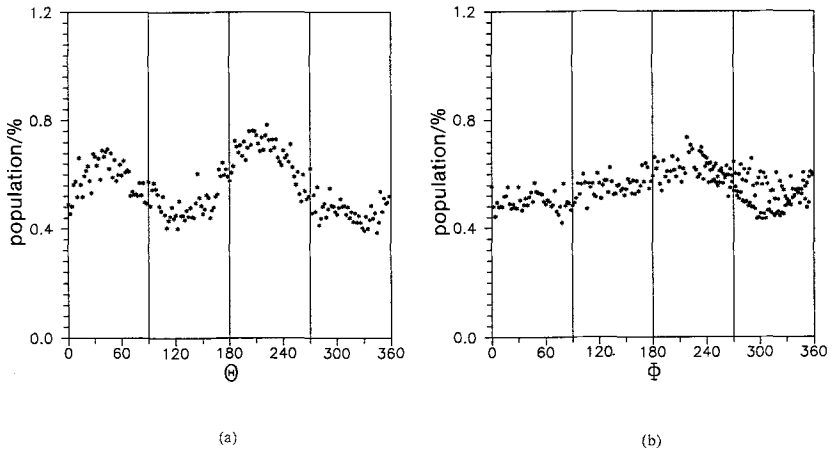

Figure 9. Histogram of percentage population of cyclohexane molecules at $\rho^* = 2{\cdot}092$ and $\gamma^* = 0{\cdot}16$ whose orientation vector $\boldsymbol{b}$ and the x-axis form an angle (*a*) Θ in the x–y plane and (*b*) Φ in the x–z plane.

ture of benzene does not account for the observed difference in viscosity between benzene and the other two fluids.

In addition to the viscosity itself, we have also examined several features of the local structure of these model fluids under shear. Figures 8 to 10 are histograms showing the percentage of molecules whose characteristic orientation vector $\boldsymbol{b}$ makes a particular angle with the x axis in either the x–y or x–z planes. We use Θ to denote the angle in the x–y plane and Φ for that in the x–z plane in the coordinate system shown in figure 2. For *n*-hexane, the orientation vector lies along the bond from site 2 to site 3; for both cyclohexane and benzene $\boldsymbol{b}$ extends from site 1 to site 4 and is thus an end-to-end vector for the hexagonal ring. As one might expect, the symmetrical ring molecules show no preferential alignment in the x–z plane—all values of Φ are equally probable. The *n*-hexane molecules, however, align roughly parallel to the flow,

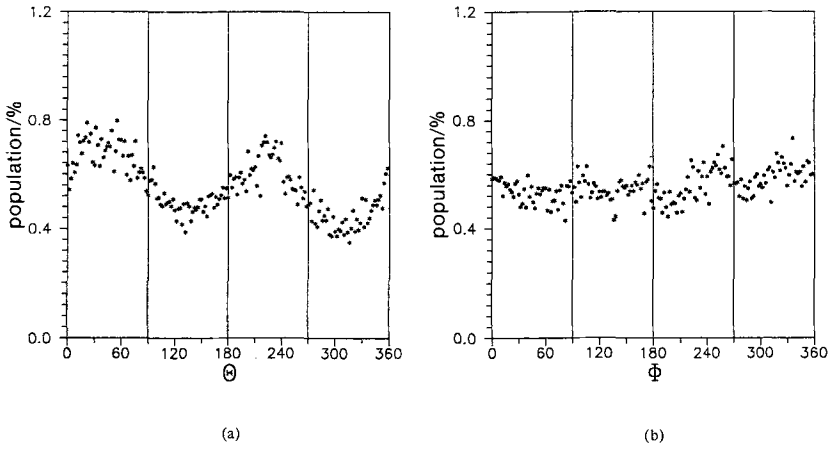

Figure 10. Histogram of percentage population of benzene molecules at $\rho^* = 2{\cdot}210$ and $\gamma^* = 0{\cdot}16$ whose orientation vector $\boldsymbol{b}$ and the x-axis form an angle (*a*) Θ in the x–y plane and (*b*) Φ in the x–z plane.

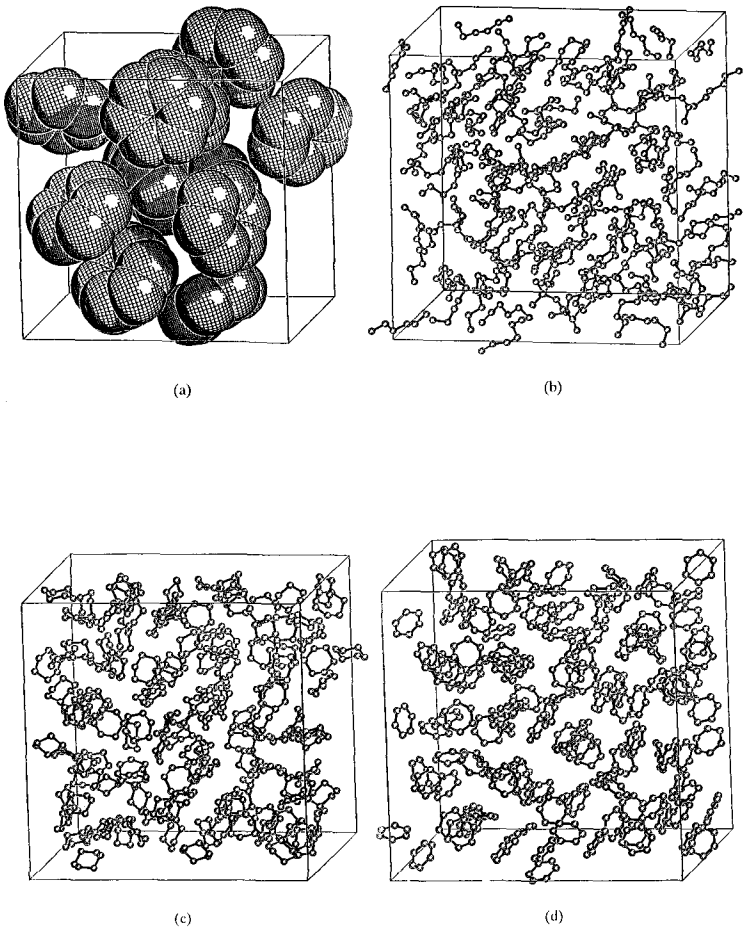

Figure 11. Snapshots of (*a*) benzene in one-eighth of simulation cell and stick-and-ball models of entire cell for (*b*) *n*-hexane, (*c*) cyclohexane and (*d*) benzene.

tending to minimize the cross-sectional area exposed to multiple shear planes. The histogram in figure 8(b) does not exhibit a 180° periodicity because of our definition of $\boldsymbol{b}$ being the 2–3 bond which is located nearer one end of the molecule than the other. The opposite end, or tail, of the molecule containing two more tetrahedral angles supplies many more opportunities for portions of the molecule to extend across shear planes, causing the tail of the molecule to drag relative to the head. This produces the lower populations observed around 180° compared to $\Theta = 0°$.

In the x–y plane, all three models show a symmetrically preferred orientation offset (about 45° in figures 8–10) from $\Theta = 0°$ and $\Theta = 180°$. This is true even for the planar benzene model. We believe this offset due to a preferential alignment of the molecules in the x–y plane with the velocity field; zero offset would correspond to the molecules lying flat and slipping past one another in planes. Much like movement of a macroscopic object through a fluid, there is a tendencey for the leading edge to lift and the trailing edge to drag. There is also evidence from animation of the simulations that the ring models tend to rotate due to the applied shear. Figure 11 (a) shows a snapshot of a cell octant during a benzene simulation. Note that some molecules are

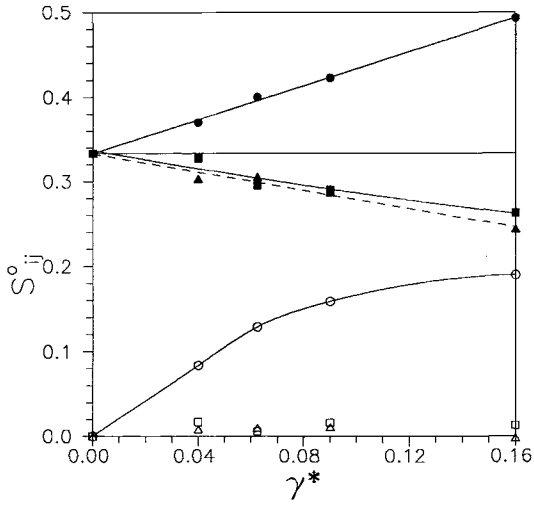

Figure 12. Components of normalized order tensor for *n*-hexane at $T^* = 4{\cdot}141$ and $\rho^* = 1{\cdot}995$. (●, S°_{xx}; ■, S°_{yy}; ▲, S°_{zz}; ○, S°_{xy}; □, S°_{xz}; and △, S°_{yz}.)

oriented at the same angle as the applied velocity field as mentioned above, and that other molecules are oriented as though tumbling or rotating like a paddle wheel in a stream. Figures 11 (b), (c) and (d) show snapshots of the entire simulation cell for the three fluids using stick-and-ball, rather than space-filling, representations to provide a clearer view of the orientations.

Molecular alignment is conveniently monitored via the symmetric order tensor

$$\mathbf{S} = \frac{1}{N}\sum_i \boldsymbol{R}_i\boldsymbol{R}_i, \tag{6}$$

where the arbitrary orientation vector $\boldsymbol{R}_i$ is taken to be the end-to-end vector. For the ring molecules $\boldsymbol{R}$ corresponds to the previously defined orientation vector $\boldsymbol{b}$. In terms of the normalized order tensor, $\mathbf{S}^\circ = \mathbf{S}/\mathrm{Tr}(\mathbf{S})$, an orientationally isotropic fluid is represented by $\mathbf{S}^\circ = \mathbf{I}/3$. Components of $\mathbf{S}^\circ$ are shown in figures 12 to 14 as a function of γ^* for the three model fluids. The tendency for the chain model to orient with the flow is clear in figure 12 and is analogous to the results obtained in [3] for *n*-butane. The symmetry of the chair model for cyclohexane apparently precludes much shear induced ordering as there will always be portions of the molecule overlapping multiple shear planes. On the other hand, the planar benzene model shows an interesting cross-over of $\mathbf{S}^\circ_{xx}$. It appears from these data that at low shear rates the benzene molecules do tend to align in stacked layers that slide over each other, but that an increase in γ^* promotes the previously mentioned rolling or tumbling motion in the x–y plane.

Information about conformational states of *n*-hexane molecules was also obtained from the simulations. Figure 15 shows a histogram of the end-to-end distances of the hexane model molecules. The maximum length corresponds to all three dihedral angles being 0°; i.e., the molecule is all *trans*. The peaks at shorter lengths correspond to the various possible combinations of *trans* and *gauche* conformations. The histogram of dihedral angles per molecule shown in figure 16 indicates that the *trans* conformation is energetically preferred by about a factor of four. It appears from this latter figure that the number of *trans*/*gauche* angles is relatively independent of the

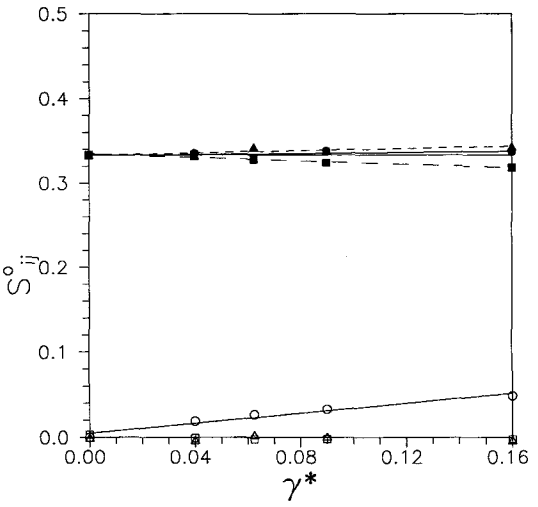

Figure 13. Components of normalized order tensor for cyclohexane at $T^* = 5{\cdot}319$ and $\rho^* = 2{\cdot}210$. See Figure 12 for symbol key.

shear rate, but is a slight function of density. There seems to be a slightly higher interconversion capability at the lower density and a slightly higher probability of the *gauche* configuration.

5. Conclusions

In this work, we have used non-equilibrium MD simulations to model the viscosity of three six-carbon liquids over a wide range of densities. Simple models containing six equivalent LJ interaction sites located at carbon centres were used to represent molecules of *n*-hexane, cyclohexane and benzene. By using the same LJ interaction parameters for all three models, only the molecular structure differs

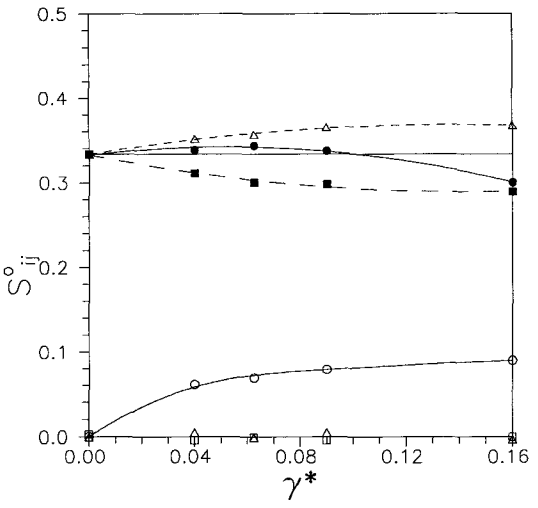

Figure 14. Components of normalized order tensor for benzene at $T^* = 5{\cdot}183$ and $\rho^* = 2{\cdot}528$. See Figure 12 for symbol key.

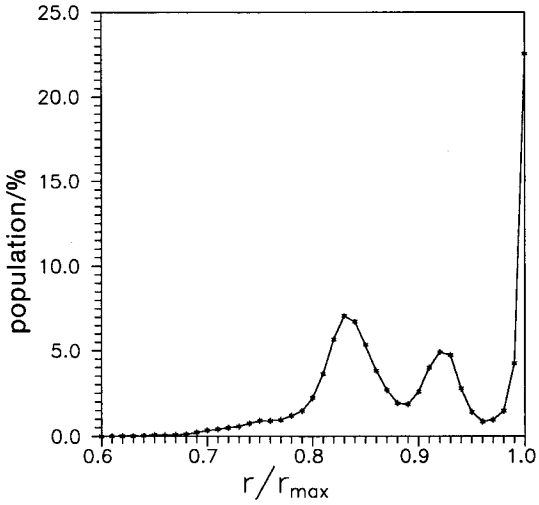

Figure 15. Histogram of end-to-end length of *n*-hexane molecules at $T^* = 4{\cdot}141$, $\rho^* = 1{\cdot}995$ and $\gamma^* = 0{\cdot}0625$.

amongst the three fluids. Simulated viscosities for the *n*-hexane and cyclohexane models agreed remarkably well with experimental data over the entire density range investigated indicating that viscosity differences in *n*-hexane and cyclohexane are structural in nature. As there are significant differences between the viscosity of straight-chain and cyclic hydrocarbons, differences which corresponding states prediction methods often fail to reproduce, it is interesting that simple site–site models can be used with the same interaction parameters to predict the fluid viscosity of either structure. This is different than the relationship between straight-chain and branched alkanes studied in [3]. There we found that structure alone did not account for the difference in viscosity, but that the site interactions themselves were slightly different.

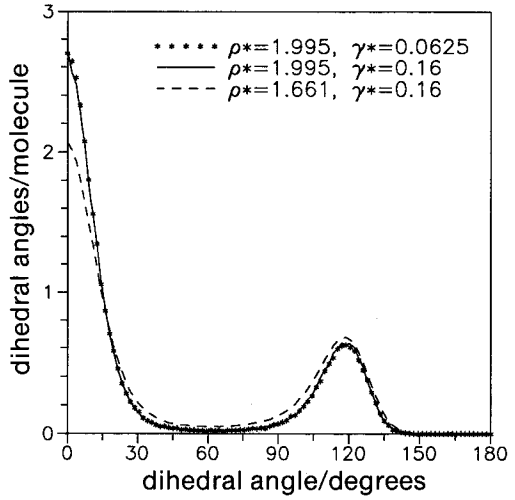

Figure 16. Histogram of dihedral angles per *n*-hexane molecule at $T^* = 4{\cdot}141$. (∗∗∗ $\rho^* = 1{\cdot}995$, $\gamma^* = 0{\cdot}0625$, —— $\rho^* = 1{\cdot}995$, $\gamma^* = 0{\cdot}16$, – – – $\rho^* = 1{\cdot}661$, $\gamma^* = 0{\cdot}16$.)

The same holds true in a comparison of simulated cyclohexane and benzene viscosities. The simulated viscosities of the planar-ring model were similar to those obtained for the chair model of cyclohexane in contradiction to the experimental trends. Experimentally, the rapid rise in benzene viscosity occurs at much higher equivalent densities than for cyclohexane. When the simulations on the benzene model fluid are performed at the higher densities where the experimental data have been measured, the model viscosity is much higher than the experimental value.

We have also examined the local structure of the model fluids under shear. We find that *n*-hexane molecules tend to align with the flow field in both the x–y and x–z planes and slide past one another like logs in a river. On the other hand, there is little alignment of the cyclohexane molecule in the shear field. Benzene molecules show the interesting feature of some stacking at lower shear rates and then tumbling at the higher shear rates.

Appendix

Using Gauss's principle of least constraint, one can write the equations of motion for sites α constrained to fixed bond angles and bond distances as [7]

$$\ddot{\boldsymbol{r}}_\alpha = \boldsymbol{F} + \sum_i \boldsymbol{M}_{\alpha n}(\lambda \boldsymbol{R}_n), \tag{7}$$

where the matrix $\boldsymbol{M}$ applies the appropriate constraints from the column vector $(\lambda \boldsymbol{R}_n)$ for each site. Here, the notation of Edberg *et al.* [7] has been retained where $\boldsymbol{R} = \boldsymbol{r}_{\alpha\beta} = \boldsymbol{r}_\beta - \boldsymbol{r}_\alpha$, with $n = \alpha + \beta - 2$ and all site masses set to unity. In this numbering scheme, nearest-neighbour vectors have odd values of n, while next-nearest-neighbour vectors have even values. The bond constraint matrices are $n_s \times n_c$, where n_s is the number of sites per molecule and n_c is the number of constraints on neighbours and next-nearest neighbours (bond angle constraints). The $\boldsymbol{M}$ matrices for the *n*-hexane, cyclohexane and benzene models used in this study are

$$\boldsymbol{M}_{\text{hexane}} = \begin{pmatrix} -1 & -1 & 0 & 0 & 0 & 0 & 0 & 0 & 0 \\ 1 & 0 & -1 & -1 & 0 & 0 & 0 & 0 & 0 \\ 0 & 1 & 1 & 0 & -1 & -1 & 0 & 0 & 0 \\ 0 & 0 & 0 & 1 & 1 & 0 & -1 & -1 & 0 \\ 0 & 0 & 0 & 0 & 0 & 1 & 1 & 0 & -1 \\ 0 & 0 & 0 & 0 & 0 & 0 & 0 & 1 & 1 \end{pmatrix}, \tag{8}$$

$$\boldsymbol{M}_{\text{cyclohexane}} = \begin{pmatrix} -1 & -1 & 0 & 0 & 0 & 0 & 0 & 0 & 0 & 1 & 1 & 0 \\ 1 & 0 & -1 & -1 & 0 & 0 & 0 & 0 & 0 & 0 & 0 & 1 \\ 0 & 1 & 1 & 0 & -1 & -1 & 0 & 0 & 0 & 0 & 0 & 0 \\ 0 & 0 & 0 & 1 & 1 & 0 & -1 & -1 & 0 & 0 & 0 & 0 \\ 0 & 0 & 0 & 0 & 0 & 1 & 1 & 0 & -1 & -1 & 0 & 0 \\ 0 & 0 & 0 & 0 & 0 & 0 & 0 & 1 & 1 & 0 & -1 & -1 \end{pmatrix}, \tag{9}$$

$$\boldsymbol{M}_{\text{benzene}} =$$

$$\begin{bmatrix}
-1 & -1 & 0 & 0 & 0 & 0 & 0 & 0 & 0 & 1 & 1 & 0 & -1 & 0 & 0 \\
1 & 0 & -1 & -1 & 0 & 0 & 0 & 0 & 0 & 0 & 0 & 1 & 0 & -1 & 0 \\
0 & 1 & 1 & 0 & -1 & -1 & 0 & 0 & 0 & 0 & 0 & 0 & 0 & 0 & -1 \\
0 & 0 & 0 & 1 & 1 & 0 & -1 & -1 & 0 & 0 & 0 & 0 & 1 & 0 & 0 \\
0 & 0 & 0 & 0 & 0 & 1 & 1 & 0 & -1 & -1 & 0 & 0 & 0 & 1 & 0 \\
0 & 0 & 0 & 0 & 0 & 0 & 0 & 1 & 1 & 0 & -1 & -1 & 0 & 0 & 1
\end{bmatrix}, \tag{10}$$

respectively.

The code used in this work was modified from the code used by Edberg *et al.* [7, 8]. We are grateful to Roger Edberg and Dennis Evans for use of their code. Gratitude is also expressed to NIST for the sabbatical opportunity of RLR and his use of the supercomputer during that time.

References

[1] Ely, J. F., and Hanley, H. J. M., 1981, *Ind. Eng. Chem. Fundam.*, **20,** 323.
[2] Okeson, K. J., and Rowley, R. L., 1991, *Int. J. Thermophys.*, **12,** 119.
[3] Rowley, R. L., and Ely, J. F., 1991, *Molec. Phys.*, **72,** 831.
[4] Ryckaert, J.-P., and Bellemans, A., 1978, *Discuss. Faraday Soc.*, **66,** 95.
[5] Jorgensen, W. L., Madura, J. D., and Swenson, C. J., 1984, *J. Am. Chem. Soc.*, **106,** 6638.
[6] Ryckaert, J.-P., and Bellemans, A., 1975, *Chem. Phys. Lett.*, **30,** 123.
[7] Edberg, R., Evans, D. J., and Morriss, G. P., 1986, *J. chem. Phys.*, **84,** 6933.
[8] Edberg, R., Morriss, G. P., and Evans, D. J., 1987, *J. chem. Phys.*, **86,** 4555.
[9] Brown, D., and Clarke, J. H. R., 1983, *Chem. Phys. Lett.*, **98,** 579.
[10] Pickett, H. M., and Strauss, H. L., 1970, *J. Am. Chem. Soc.*, **92,** 7281.
[11] Kuharski, R. A., Chandler, D., Montgomery, Jr., J. A., Rabii, F., and Singer, S. J., 1988, *J. phys. Chem.*, **92,** 3261.
[12] Hoheisel, C., and Würflinger, A., 1989, *J. chem. Phys.*, **91,** 473.
[13] Evans, D. J., and Watts, R. O., 1976, *Molec. Phys.*, **32,** 93.
[14] Steinhauser, O., 1982, *Chem. Phys.*, **73,** 155.
[15] Ciccotti, G., Ferrario, M., and Ryckaert, J.-P., 1982, *Molec. Phys.*, **47,** 1253.
[16] Claessen, M., Ferrario, M., and Ryckaert, J.-P., 1983, *Molec. Phys.*, **50,** 217.
[17] Linse, P., 1984, *J. Am. Chem. Soc.*, **106,** 5425.
[18] Linse, P., Engström, S., and Jönsson, B., 1985, *Chem. Phys. Lett.*, **115,** 95.
[19] Karlström, G., Linse, P., Wallqvist, A., and Jönsson, B., 1985, *J. Am. Chem. Soc.*, **105,** 3777.
[20] Maliniak, A., and Laaksonen, A., 1987, *Molec. Phys.*, **62,** 489.
[21] Yashonath, S., Price, S. L., and McDonald, I. R., 1988, *Molec. Phys.*, **64,** 361.
[22] Anderson, J., Ullo, J. J., and Yip, S., 1987, *J. chem. Phys.*, **86,** 1987.
[23] Gupta, S., Sediawan, W. B., and McLaughlin, E., 1988, *Molec. Phys.*, **65,** 961.
[24] Evans, D. J., and Morriss, G. P., 1984, *Phys. Rev. A*, **30,** 1528.
[25] Evans, D. J., and Morriss, G. P., 1984, *Comput. Phys. Rept.*, **1,** 297.
[26] Ryckaert, J.-P., Ciccotti, G., and Berendsen, H. J. C., 1977, *J. Comput. Phys.*, **23,** 327.
[27] Evans, D. J., Hoover, W. G., Failor, B. H., Moran, B., and Ladd, A. J. C., 1983, *Phys. Rev. A*, **28,** 1016.
[28] Rowley, R. L., and Ely, J. F., 1991, *Molec. Simulation*, **7,** 303.
[29] Dymond, J. H., Young, K. J., and Isdale, J. D., 1980, *Int. J. Thermophys.*, **1,** 345.
[30] Jonas, J., Hasha, D., and Huang, S. G., 1980, *J. phys. Chem.*, **84,** 109.
[31] Dymond, J. H., Robertson, J., and Isdale, J. D., 1981, *Int. J. Thermophys.*, **2,** 223.